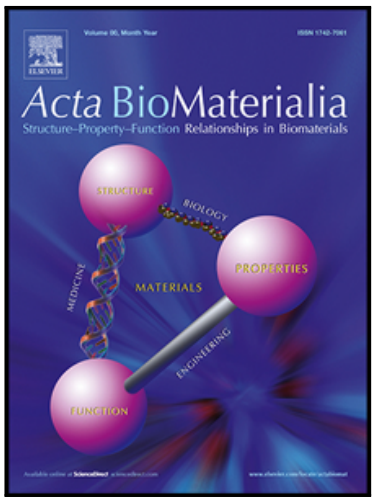


# Equilibrium interactions of biomimetic DNA aptamers produce intrafibrillar calcium phosphate mineralization of collagen

Kassidy Patoine , Kristy Ta , Amanda Gilbert , Marielle Percuoco , Aren E. Gerdon

PII: S1742-7061(24)00146-6
DOI: https://doi.org/10.1016/j.actbio.2024.03.018
Reference: ACTBIO 9240

To appear in: *Acta Biomaterialia*

Received date: 10 November 2023
Revised date: 13 March 2024
Accepted date: 18 March 2024

Please cite this article as: Kassidy Patoine , Kristy Ta , Amanda Gilbert , Marielle Percuoco , Aren E. Gerdon , Equilibrium interactions of biomimetic DNA aptamers produce intrafibrillar calcium phosphate mineralization of collagen, *Acta Biomaterialia* (2024), doi: https://doi.org/10.1016/j.actbio.2024.03.018

# Equilibrium interactions of biomimetic DNA aptamers produce intrafibrillar calcium phosphate mineralization of collagen

*Kassidy Patoine*[1], *Kristy Ta*[1], *Amanda Gilbert*[1], *Marielle Percuoco*[1], *Aren E. Gerdon*[1]*

1. Department of Chemistry & Physics, Emmanuel College, 400 Fenway, Boston, MA 02115

KEYWORDS: collagen, DNA aptamer, mineralization, bone

*Corresponding Author email: gerdoare@emmanuel.edu, phone: 617-735-9769



Abstract

Native and biomimetic DNA structures have been demonstrated to impact materials synthesis under a variety of conditions but have only just begun to be explored in this role compared to other biopolymers such as peptides, proteins, polysaccharides, and glycopolymers. One selected DNA aptamer has been explored in calcium phosphate and calcium carbonate mineralization, demonstrating sequence-dependent control of kinetics, morphology, and crystallinity. This aptamer is here applied to a biologically-relevant bone model system that uses collagen hydrogels. In the presence of the aptamer, intrafibrillar collagen mineralization is observed compared to negative controls and a positive control using well-studied poly-aspartic acid. The mechanism of interaction is explored through affinity measurements, kinetics of calcium uptake,

and kinetics of aptamer uptake into the forming mineral. There is a marked difference observed between the selected aptamer containing a G-quadruplex secondary structure compared to a control sequence with no G-quadruplex. It is hypothesized that the equilibrium interaction of the aptamer with calcium-phosphate precursors and with the collagen itself leads to slow kinetic mineral formation and a morphology appropriate to bone. This points to new uses for DNA aptamers in biologically-relevant mineralization systems and the possibility of future biomedical applications.

## 1. Introduction

Bone is a complex biomaterial that requires the hierarchical assembly of collagen protein, inorganic mineral, and other components on many different scale levels.[1] Biological bone formation, including structure and function,[1,2] and biomimetic control of bone repair[2–11] has been studied to a large extent over the past decades and continues to attract research attention due to the complexity of the material and biological environment and the need for restorative procedures. Systems studied have included animal models, demineralized tendon or enamel, and assembled collagen hydrogels that present networks and arrays of organized collagen fibrils. In vitro mineralization of collagen requires three essential factors which include the collagen itself, the forming mineral, and a non-collagenous protein (NPC) mimic or additive.[12] Biomimetic macromolecules serve as analogs to the NCPs typically expressed in the extracellular matrix in a biological environment and could prove useful as controllable, synthetic, and available treatments in biomedical bone remineralization. One well-studied NCP analog is poly-aspartic acid (pAsp),[2,4,13] chosen for the low pKa of the carboxylic acid side chains that results in a high negative charge and strong ability to chelate metal cations. Its homopolymeric nature also

provides a general lack of secondary structure making pAsp a non-rigid and adaptable biomolecule. A wide range of evidence has demonstrated the usefulness of pAsp in promoting biologically-relevant internal mineralization of collagen fibrils, known as intrafibrillar mineralization, creating a mechanically strong material. This action has been demonstrated to follow a polymer-induced liquid precursor (PILP)[2,3,6,13–18] mechanism where the pAsp forms liquid-phase associations with calcium and phosphate ions that are fluid, quasi-stable, and amorphous in crystallinity and morphology. It has been proposed that through capillary action these PILP associations are transported into the collagen fiber where they later form crystalline hydroxyapatite (HAP). The mechanism behind the transition from an amorphous to crystalline phase remains poorly understood and may involve other intermediate phases.[12] While numerous experiments have provided insight into the PILP mechanism, research interest in this area remains a priority for understanding, controlling, and recreating the impressive hierarchical structure of bone. One important consideration is in the structure-function relationship for pAsp in this role as an NCP mimic and if there are other biomacromolecules that could provide additional advantages in mineralization.

DNA and RNA are biomacromolecules with a multitude of functions and roles in biology and biomimetics. Both have intended functions in the body but have also been shown to have unexpected effects related to calcium mineral formation in disease states or following cell apoptosis indicating a potential natural, though often overlooked, connection between DNA and mineral.[19–21] This connection has recently been highlighted by showing that large (15-30 kbp) DNA sequences extracted from natural tissues can influence intrafibrillar collagen mineralization, suggesting that DNA in vivo could play a role in pathological mineralization or could be leveraged to improve bone regeneration.[21] Similarly, large, native DNA and RNA sequences have been integrated with calcium phosphate mineral to make composites used in

vector delivery[22] and immuno-modulatory bone repair,[23] demonstrating the potential biomimetic effect on biological activity. On a molecular level, DNA is a polymer with an extended phosphate backbone, an ability to chelate divalent cations, potential for unique secondary structures, and exceptional programmability in base-pairing when known sequences are prepared and optimized. Designer DNA origami structures of various shapes and patterns have been shown to direct calcium phosphate precursors to promote controlled mineralization offering potential in biomimetic hierarchical materials.[24–30] Smaller, synthetic DNA and RNA aptamers have been widely studied for their biomimetic capabilities that mirror enzyme-like catalysis and antibody-like affinity[31–33] but have only recently been explored related to materials affinity or as templates in materials synthesis.[34–42] In particular, the Liu group has demonstrated interactions between short oligonucleotides and metal oxide or metal phosphate materials[37,39,40] while Bawazer, et al.[34] selected a DNA aptamer for ZnO formation.

We previously reported a novel Precipitation SELEX[43] (Systematic Evolution of Ligands by Exponential Enrichment) method that resulted in the identification of a DNA aptamer with an ability to influence calcium phosphate mineralization in vitro. It was found that this 40-nucleotide aptamer (Aptamer G, 12.5 kDa) contains a hybrid or 3+1 G-quadruplex secondary structure[44,45] and that the adaptability of that structure leads to control of mineralization kinetics, morphology, and crystallinity under various conditions with both calcium phosphate and calcium carbonate precursors.[43,44,46] A control sequence (Aptamer G-, 12.5 kDa) has the same number of nucleotides and similar sequence as Aptamer G but is mutated to prevent G-quadruplex formation. Circular dichroism (CD) experiments have previously confirmed the presence of a G-quadruplex structure in Aptamer G and a lack thereof in Aptamer G-.[44] CD has also demonstrated a significant interaction of Aptamer G with calcium ions compared to Aptamer G-,[44] which has been supported by DNA melt temperature experiments in the presence of calcium

ions from 0.5 μM to 2 mM. Aptamer G appears to be more sensitive to calcium ion concentration compared to Aptamer G-, indicating a stronger interaction between the G-quadruplex structure and the calcium ion.[46] Fluorescence measurements have shown lower stability of Aptamer G at higher pH compared to Aptamer G- as well.[44] Based on these previous results, Aptamer G appears to form a less rigid and more adaptable secondary structure while Aptamer G-, capable of forming canonical base-pairing, produces a more rigid hairpin-loop structure. These differences in structure, stability, and adaptability have been shown to play an important role in the function of the aptamers. Similar poly-anionic proteins and polymers, such as pAsp, have undefined, globular structures and have been used to demonstrate biomimetic control of calcium phosphate mineralization of collagen hydrogels through PILP mechanism.[2,13] It is hypothesized that Aptamer G could perform in a similar PILP mechanism to pAsp but could also present new opportunities due to the poly-phosphate backbone and uniquely programmable primary and secondary structure not possible with pAsp or with large, native DNA sequences. In this work, we aim to elucidate the influence of Aptamer G on collagen mineralization in comparison to known pAsp and to Aptamer G-. This demonstrates the usefulness of DNA aptamers in biologically- and medically-relevant biomaterials synthesis and helps to expand the use of DNA aptamers in more complex biological systems.



## 2. Materials and Methods

2.1 *Chemicals*. Type I Bovine collagen (Telocol-3, 3.1 mg/ml) was purchased from Advanced Biomatrix. Poly-aspartic acid (PLD200, 27 kDa) was purchased from Alamanda Polymers. Tris hydrochloric acid (99.0%), sodium phosphate dibasic (99.0%), calcium chloride anhydrous (99.5%), sodium borohydride (98%), and L-glutathione reduced (>98 %) were purchased from Sigma Aldrich. Strontium AAS standard solution (1000 μg/mL) and sodium azide were

purchased from Thermo Fisher Scientific. A 10x tris borate EDTA (TBE) buffer was purchased from Bio-Rad. GelStar Nucleic Acid Gel Stain was purchased from Lonza. Hydrogen tetrachloroaurate (99.9 %) was purchased from Strem Chemicals. DNA strands were purchased from Integrated DNA Technologies and were reconstituted in 10 mM tris buffer pH 7.4 before use. Synthesis and purity were confirmed by the vendor using mass spectrometry. UV absorbance was used to confirm concentration of DNA. Aptamer were annealed at 85-95 $^{o}$C in 50.0 mM tris pH 7.4, 150 mM sodium chloride, 4.5 mM calcium ion and cooled to room temperature before each experiment. The following ssDNA aptamers were used for analysis: (Aptamer G, 12.5 kDa) 5′-CAG GTG GGC GCG CTG TCG TGC GTG CTC GGG TGC GGT TGG G− 3′; (Aptamer G−, 12.4 kDa) 5′-CAG GTG CGC GCG CTG TCG TGC GTG CTC GCG TGC GGT TGC G− 3′; (Aptamer $G_L$) 5’-AAA AAA AAA AAA CAG GTG GGC GCG CTG TCG TGG GTG CTC GGG TGC GGT TGC G− 3′; (T12-linker) 5′-TTT TTT TTT TTT-3′-$C_3H_6$-SH. All solutions were filtered prior to use and fresh mineralization solutions were prepared each day.

2.2 *Collagen Hydrogel Preparation*. Collagen hydrogels were prepared by combining 1200 µL Type I bovine collagen (3.1 mg/mL), 300 µL 10x phosphate-buffered saline (PBS), and 200 µL 0.1 N NaOH, followed by ice-bath sonication for five minutes and incubation at 37°C for one hour. Hydrogels were rinsed with deionized (DI) water twice, then once with tris buffer prior to use. Hydrogel preparations were reproducible with consistent size, shape, and mass.

2.3 *Mineralization and Analysis of Collagen Hydrogels*. Collagen hydrogels were incubated at 37 $^{o}$C in mineralization solution containing 50.0 mM tris pH 7.4, 150 mM sodium chloride, 0.02% sodium azide, 4.5 mM calcium ion, and 2.1 mM phosphate ions.[3] These conditions produce an oversaturation with respect to hydroxyapatite (HAP) with a saturation index of 11.97

as calculated using Visual MINTEQ Ver 3.1.[47] Biomimetic polymers were added to 1.8 μM and included either poly-aspartic acid, Aptamer G, Aptamer G-, or a control with no added polymer. Solutions reacted at 37 °C with rotation for 1-15 days. Mineralized hydrogels were then rinsed in DI water, frozen in dry ice-acetone, and lyophilized in vacuum. Lyophilized samples were analyzed in several ways including FT-IR using a Thermo Nicolet Avatar 370 instrument with Si10 ATR at 64 scans and 4 $cm^{-1}$ resolution. SEM was used after sputter-coating with 4.5 nm Pt using a Leica EM ACE600 and a Hitachi-S-4700 SEM at 3 or 5 kV. TEM was used after shredding collagen fibers, rehydrating in water, spotting on a grid and air drying, using 200-mesh Cu Formvar grids and a JEOL 1200EX 80 kV instrument. Alternatively, according to published methods,[7,21,30] collagen was combined with 10x PBS and 0.1 N NaOH as described above, then 2 μL was added directly to a 200-mesh Ni Formvar TEM grid and incubated at 37 °C for 1 h. The TEM grid was rinsed in DI water then floated with the collagen-side-down on 30 μL of the mineralization solution described above. This was placed in a humid chamber at 37 °C and incubated for 3 days. The grid was then washed in DI water and dried prior to TEM analysis.

2.4 *Calcium Uptake During Mineralization*. Concentration of calcium in the mineralization solution was measured during the mineralization process in two ways. A calcium ion selective electrode (Cole-Parmer) was calibrated and used to measure calcium directly in the mineralization solution at various timepoints during the reaction. Samples were removed from incubation and cooled to room temperature for measurement then returned to incubation at 37 °C. A calibration curve was prepared at each measurement timepoint using a range of standard calcium solutions. Calcium concentration in each unknown solution was determined through the calibration curve and error was propagated through regression analysis and reported as standard deviation. Inductively-coupled plasma atomic emission spectroscopy was used to measure

calcium in triplicate in aliquots removed from the reaction solutions. Standard calcium solutions were combined with a strontium internal standard and measured to establish a calibration between the two. At each timepoint, 100 μL aliquots of mineralization solution with 100 μL of 100.0 ppm strontium standard and 1.0 mL of 1.0 M nitric acid were combined and diluted to 10.0 mL prior to analysis on an Agilent MP-4100 AES instrument at 393.366 nm and 407.771 nm for calcium and strontium respectively.

2.5 *DNA Aptamer Uptake During Mineralization*. Concentration of aptamer in the mineralization solution was measured during the mineralization process using fluorescence. A sample with DNA aptamer in tris buffer with no calcium, phosphate, or collagen was used as a control. At each time point, 10 μL aliquots of mineralization solution were diluted in triplicate in 1x TBE buffer with 1x Gelstar dye. Fluorescence was measured on a Horiba Fluoromax-3 with excitation at 493 nm with 5 nm slit width and emission from 500-600 nm with 1 nm slit width.

*2.6 Analysis of Particle Size During Mineralization*. Particle size was measured in triplicate using dynamic light scattering and a Wyatt DynaPro Nanostar DLS. Ten microliter aliquots were removed from the mineralization supernatant and analyzed in triplicate at 20 $^{o}$C.

2.7 *DNA Aptamer Affinity for Collagen*. Collagen hydrogels were prepared as above but on a smaller 1:10 scale. Concentrations of Aptamer G and Aptamer G- from 0.2 to 8 μM were annealed in tris buffer pH 7.4 with 4.5 mM calcium ions for 10 minutes at 85°C, then cooled to room temperature. The annealed DNA samples were added to the hydrogels and reacted for one hour at 37°C in tris buffer pH 7.4 with 4.5 mM calcium ions. Samples were centrifuged for one minute and supernatant aliquots were analyzed in triplicate for absorbance at 260 nm using an

Agilent 8453 UV-Vis spectrophotometer. An equilibrium constant was calculated for Aptamer G following the Langmuir isotherm, described in Supporting Information **S4**.

2.8 *Mineralization of Collagen Hydrogels with Gold Nanoparticle Labeling*. Mineralization of collagen with Aptamer G was completed as above but with 1.78 μM Aptamer G, 0.02 μM Aptamer $G_L$, and 0.02 μM functionalized gold monolayer-protected nanoparticle. The nanoparticle was synthesized and functionalized according to prior work.[48–51] Briefly, 0.3 mmol auric acid was combined with 0.9 mmol glutathione in 25 mL cold ethanol with 10 mL cold DI water. Sodium borohydride (3 mmol) was dissolved in 5 mL water DI water and added rapidly to the gold-glutathione solution to produce a characteristic dark nanoparticle suspension. The sample was precipitated in ethanol and impurities decanted prior to dissolving in DI water and placing in dialysis (13 kDa MWCO) for three days, changing the water daily. Resulting monolayer-protected nanoparticles were dried and analyzed by NMR (Anasazi 90 MHz, in $D_2O$), DLS (Wyatt Instruments), and TEM (JEOL 1200EX-80 KV). T12-linker DNA was attached by place exchange in buffer (4 mM phosphate pH 7.4, 2 M sodium chloride, 12.5 mM magnesium chloride) by stirring at room temperature for 24 h. Nanoparticle with attached T12-linker was purified from free linker with a 10 kDa MWCO spin filter (Amicon) and confirmation of T12-linker attached was obtained by absorbance measurement of the eluent compared to a control. Aptamer $G_L$ was added at a 1:1 aptamer to nanoparticle ratio, annealed to 50 $^oC$, and cooled to 37 $^oC$ prior to addition to mineralization. Resulting mineralized hydrogels were analyzed with SEM and TEM as described above.

2.9 *Statistical Analysis*. Several methods of statistical analysis were employed throughout this work. In Supporting Information S2, error bars from replicate measurements of fiber widths represent standard deviations. An unpaired t-test was conducted to determine statistical

significance between different samples and p-values are provided. Statistical significance threshold was set at 95% confidence or $P < 0.05$. In calcium uptake experiments, Figure 3A, calcium concentration in each unknown solution was determined through the calibration curve and error was propagated through regression analysis and reported as standard deviation. An unpaired t-test was used to compare data points at different timepoints and results are reported as p-values. Statistical significance threshold was set at 95% confidence or $P < 0.05$. In DNA aptamer affinity experiments, Figure 3B, and DNA aptamer uptake experiments, Figure 3C, error bars from replicate measurements represent standard deviations. In DNA affinity experiments, an equilibrium constant was calculated for Aptamer G following the Langmuir isotherm, described in Supporting Information S4. Error was propagated through regression analysis of the linearized version of the Langmuir isotherm model and reported as the standard deviation of the equilibrium constant. In DNA aptamer uptake experiments, unpaired t-tests were used to compare data points at different timepoints and results are reported as p-values. Statistical significance threshold was set at 95% confidence or $P < 0.05$.



## 3. Results and Discussion

DNA Aptamer G, selected for an ability to interact with calcium phosphate mineral precursors, has a known primary sequence and a non-rigid G-quadruplex secondary structure. Here we demonstrate the influence of Aptamer G on intrafibrillar collagen mineralization and highlight the difference between it and a control aptamer sequence, Aptamer G-. Collagen hydrogels were prepared by neutralizing soluble Type I collagen with incubation at 37 $^{o}$C, producing samples of consistent mass, size, and shape. Mineralization conditions followed previously reported conditions using low concentrations of calcium ions at 4.5 mM and phosphate ions at 2.1 mM,

incubation at 37 $^{o}$C, and agitation using a rotational shaker or with no agitation in experiments on TEM grids. Enhanced mineralization kinetics, producing more mineral in a shorter period of time, could have been achieved with higher ion concentrations or more aggressive solution mixing. Since the goal of this work is to understand the influence of DNA aptamers on collagen mineralization, modest levels of mineralization were more desirable than collagen overloaded with mineral. Under these milder mineralization conditions some amount of heterogeneity in mineral formation was expected while clear trends developed.

Apparent differences in mineralization are observed in TEM and SEM images at different timepoints in Figure 1, when Aptamer G, Aptamer G- or no aptamer was added to solution. Figures 1a,b, 1g,h, and 1m,n show TEM images from mineralization experiments conducted directly on collagen-coated TEM grids for 3 days. Figure 1a, with no aptamer added, shows large, 5 μm spherical-like mineral particles formed either independent of collagen fibers or adjacent to fibers. Figure 1b, from the same sample, shows what appears to be mineral forming around collagen fibers but not within fibers, which is expected when no NCP or NCP-mimic is present. Figure 1g, with Aptamer G present, shows smaller, 1-2 μm, mineral particles that appear more bundle-like than spherical and are more intimately connected throughout long collagen fibers. Figure 1h shows higher magnification of collagen that appears in the process of intrafibrillar mineralization with mineral stretching along the long axis of the fiber. Figure 1m, with Aptamer G- present, shows larger, 5-10 μm, spherical-like mineral particles that appear to be surrounded by external collagen fibers and that are similar in shape to that in Figure 1a with no added aptamer. Figure 1n at higher magnification does show small mineral particles associating with the collagen but in a less organized fashion compared to that in Figure 1h.

Aptamer G- may be helping to bring mineral to the collagen fibers but not in a manner that appears consistent with intrafibrillar mineralization.

Using SEM, larger collagen hydrogel samples could be analyzed. Experiments with Aptamer G present show minor signs of external, surface mineralization after 7 days in Figure 1i but primarily show thick collagen fiber bundles that are suggestive of internal, intrafibrillar mineralization. Some fibers demonstrate smooth, mineralized bundles in Figure 1j while others contain a crystalline mineral morphology or bristling fibers in Figure 1j,k. After 14 days of reaction, in Figure 1l, mineral still appears to be aligned with collagen fibers with additional mineral forming clusters. The presence of thick, bristling fibers in SEM images adds support to the conclusion that intrafibrillar mineralization is occurring in the presence of Aptamer G. This is consistent with SEM images, seen in Supporting Information S2, from mineralization experiments using pAsp as a positive control since it is known to produce intrafibrillar mineralization.[13] This type of mineralization is not observed in control experiments with no DNA aptamer in Figure 1c-f or with Aptamer G- in Figure 1o-r. The difference between mineralization with Aptamer G compared to Aptamer G- or no DNA aptamer is apparent in all images. Aptamer G- shows fibers that are thin and unmineralized with particles of crystalline mineral lodged between fibers in Figure 1o. The results for Aptamer G- are similar to those when no DNA aptamer is used in the control in Figure 1c-f. After 14 days mineral formed with no aptamer in Figure 1f and with Aptamer G- in Figure 1r both show crystalline, plate-like mineral with collagen fibers weaved between mineral, which is not consistent with intrafibrillar mineralization. Fiber thickness measured in 7-day SEM experiments using image analysis further supports the conclusion of intrafibrillar mineralization. Fiber thickness is statistically different ($P < 0.0001$) with $260 \pm 20$ nm diameter fibers measured when Aptamer G is used and $160 \pm 20$ nm diameter fibers measured when no aptamer additive is included. Furthermore, there is no

statistical difference ($P > 0.39$) between fiber diameters when Aptamer G is used compared to pAsp, shown in Supporting Information S1. Additional TEM and SEM images, including comparison images when poly-aspartic acid additives were used can be found in Supporting Information S2.

FT-IR spectroscopy analysis using attenuated total reflectance of the mineralized collagen showed significant peaks for amide functional groups found in collagen at 1632 $cm^{-1}$ and for phosphate at 1016 $cm^{-1}$, 557 $cm^{-1}$, and 598 $cm^{-1}$ in Figure 2, which confirms the presence of calcium phosphate mineral in the collagen sample.[46,52,53] A crystallinity factor, Cf, which describes progression towards crystalline mineral can be determined, as described by Choi, et al.[53] by using peaks at 557 and 598 $cm^{-1}$ and valleys at 587 $cm^{-1}$ as $(I_{557} + I_{598})/I_{584}$ after normalization. HAP standards typically have Cf values ranging from 5 to 13.[46,53] Heterogeneity of the mineralized collagen samples was observed within a single sample and between samples, shown in Figure 2 and Supporting Information S3, where Cf values ranged from 2.0 to 3.2. Figure 2 shows three representative spectra from three different collagen samples each mineralized in the presence of Aptamer G for 7 days. Variability in crystallinity can be observed in the definition of phosphate peaks at 1016, 557, and 598 $cm^{-1}$. As such, no clear trend was observed in mineral crystallinity or in the ratio of peak intensity for phosphate compared to amide when considering sample mineralized with poly-aspartic acid, Aptamer G, Aptamer G-, or in the absence of aptamer. It was noted that mineral crystallinity appeared to increase when the ratio of phosphate to collagen also increased, shown in Supporting Information S3, but this does not indicate intrafibrillar mineralization on its own because uncontrolled surface mineralization is also likely to be crystalline. This can be observed in crystalline-like morphology of mineral that is independent of collagen fibers formed in the control sample in Figure 1. Intrafibrillar mineral observed in SEM and TEM images in the presence of Aptamer G appears to be

crystalline in some areas and potentially amorphous in other areas which agrees with the FT-IR results. Under these reactions conditions, different portions of the collagen hydrogel may mineralize and transform to crystalline material at different rates potentially due to quality of the fiber formation, lower calcium and phosphate supersaturation conditions, accessibility to mineralization solution, or the low 1.8 μM concentration of aptamer used.

The kinetics of mineral formation with each aptamer was followed over a 14-day period by measuring calcium ion concentration in the supernatant solution. A calcium ion-selective electrode was used for supernatant measurements and demonstrated the influence of Aptamer G and Aptamer G- on mineralization kinetics in Figure 3A. Control samples with no collagen present in buffer with free calcium ions and either Aptamer G or Aptamer G- showed minimal variability in measured signal over 14 days indicating the stability of the measurement and an inability of low 1.8 μM concentrations of aptamer to influence higher 4.5 mM concentrations of free calcium ions. Control samples with collagen hydrogels, free calcium ions, and no aptamer showed calcium ion uptake by the collagen independent of any mineralization or aptamer interaction. Nearly 5 +/- 2 % of calcium ions were sequestered by the collagen, likely through electrostatic interactions, for the 14 days. Mineralization of the collagen hydrogel in the absence of any aptamer additive showed calcium ion uptake within the first three days of reaction and continued until more than 50% of calcium ion had been removed from solution. This might include some amount of bulk precipitation in solution but also includes surface mineralization of the collagen hydrogel. Inclusion of Aptamer G and Aptamer G- both demonstrated a delay or inhibition of calcium ion uptake, with Aptamer G showing the greatest effect. After 7 days of mineralization, calcium uptake when either Aptamer G or Aptamer G- was statistically different from the No Aptamer control ($P < 0.0005$). After 14 days of mineralization, calcium uptake with

Aptamer G present was statistically different from both Aptamer G- and the No Aptamer control ($P < 0.05$). This would indicate that Aptamer G is potentially interacting with the calcium and phosphate precursors in solution to a greater degree or with greater affinity than Aptamer G-, preventing bulk mineralization, and promoting intrafibrillar mineralization seen in Figure 1. The kinetic inhibition observed with Aptamer G- may be following a different mechanism of interaction with mineral precursors that does not delay particle nucleation and growth to as great of an extent and does not encourage precursor association with collagen fibrils.

The role of the DNA aptamer, its interaction with collagen and with mineral precursors, was further investigated through absorbance, fluorescence, and dynamic light scattering experiments to track aptamer in solution. The affinity of each DNA aptamer to collagen in the presence of calcium ion, but the absence of phosphate, was determined through solution absorbance experiments. The absorbance of each aptamer in solution decreased when incubated with collagen hydrogels at 37 $^{o}$C for 30 min, presumably due to adsorption of the aptamer to the collagen. Increasing the concentration of aptamer in solution led to an increase in adsorption for both aptamers but in very different ways in Figure 3B. Aptamer G showed an increase in binding to the collagen with binding saturation at higher micromolar concentrations, indicating adsorption behavior that could be modeled with a Langmuir isotherm.[54,55] The isotherm assumes monolayer adsorption at equilibrium and indicates a dissociation constant ($K_d$) of 2.5 $\pm$ 0.7 μM. The Langmuir isotherm calculation and fit are available in Supporting Information S4. Aptamer G- shows a linear increase in binding with increasing concentration. This does not indicate monolayer formation at equilibrium but rather suggests non-specific adsorption that might include multi-layer aggregation. Since both aptamers have the same number of nucleotides and

similar overall charge, the interaction with calcium and collagen must be dominated by the aptamer secondary structure, resulting in very different binding interactions.

Analogous experiments were performed in the presence of mineralization solution over the course of 14 days in Figure 3C. Throughout the mineralization reaction, aliquots of supernatant were removed, combined with Gel Star dye, and analyzed with fluorescence spectroscopy. Aptamer dissolved or suspended in solution, not associated with collagen, would be collected and detected in fluorescence measurements. Control experiments using DNA aptamers with calcium ion but in the absence of phosphate or collagen show that the aptamers are stable and are not degraded in this mineralization environment shown in Supporting Information S5. Removal of aptamer from solution is therefore presented as the percent of aptamer uptake, which could include affinity binding to collagen, like seen in Figure 3B, or could include participation or entrapment in forming mineral precursors associated with collagen. Both Aptamer G and Aptamer G- demonstrate initial uptake in the first 2-24 hrs, ranging from 6 to 12% uptake, that is likely associated with adsorption to the collagen possibly in complexation with calcium or calcium phosphate precursor. While the amount of uptake is similar between the two aptamers at this point, the interaction with the collagen could be quite different based on the affinity results in Figure 3B. As time continues Aptamer G- remains stably associated with the collagen, ranging from 10 to 12% uptake. After approximately 7 days calcium uptake due to mineralization increases dramatically, as observed in Figure 3A, and corresponds to a similar increase in uptake for Aptamer G- reaching nearly 80% uptake. Inhibition of mineral formation by Aptamer G- persists for approximately 7 days at which point mineral growth apparently overcomes the influence of the aptamer. It is likely that Aptamer G- is then enveloped by or adsorbed to the surface of mineral growing between collagen fibrils seen in Figure 1, consistent with previous findings that Aptamer G- has an affinity for calcium phosphate.[46]

Aptamer G shows a different impact on collagen mineralization. Affinity of Aptamer G to the collagen surface appears to be equilibrium driven in Figure 3B and that equilibrium may be shifting during the subsequent days of mineralization. Uptake or affinity of Aptamer G drops to nearly zero after 2 to 3 days indicating that the concentration of free aptamer in solution has increased possibly due to complex formation with networks of calcium phosphate precursors rather than with collagen. After 5 to 7 days aptamer uptake begins to rise, reaching a plateau of 16 to 19% uptake at the same time that calcium uptake in Figure 3A begins to rise. This indicates mineralization inhibition, the slow transport of aptamer and calcium ions into the collagen, and results in intrafibrillar mineralization seen in Figure 1. Presumably, calcium ion uptake and Aptamer G uptake would continue to rise slowly as intrafibrillar mineralization proceeded and eventually transitioned to external, bulk mineralization. At both 7 and 14 days of mineralization, the percent of aptamer uptake for Aptamer G is statistically different from that of Aptamer G- ($P < 0.0005$).

Dynamic light scattering analysis of particles in solution at 4 h and 14 d show a wide range of particles sizes spanning 7-12 nm, 100-400 nm, and 900-16000 nm when % intensity is plotted in Supporting Information S6. This wide range of particles sizes could be due to the heterogeneity of the solution or the low 1.8 μM concentration of aptamer, already discussed. When focusing on the smaller size range that is likely to include aptamer and PILP-like materials, Aptamer G shows 6 $\pm$ 1 nm particles at 4 h and 12 $\pm$ 3 nm particles at 14 days. Aptamer G- shows consistent 5 $\pm$ 1 nm particles at both 4 h and 14 days. This agree with results above that Aptamer G may be changing its interaction with calcium phosphate precursors over time due to shifts in equilibrium but Aptamer G- has a static interaction.

In order to track the location of Aptamer G after 7 days of mineralization, 2 nm diameter gold nanoparticles were employed as markers detectable in TEM. Aptamer G was used at a total concentration of 1.8 μM, in line with all previous experiments, but 1% of this aptamer contained a 5'-$A_{12}$ sequence that hybridized to a 3'-thiolated $T_{12}$ sequence attached to a gold nanoparticle. We hypothesize that the native aptamer and the nanoparticle-tagged aptamer would both participate in the mineralization process as in previous experiments, allowing for identification

of the location of aptamer in the collagen sample. TEM analysis of the mineralized collagen in Figure 4 shows well-defined collagen fibrils, mineral that appears to be both internal and external to the fibril, and gold nanoparticles that appear to be closely associated with the fiber. Nanoparticles are not associated with external mineral particles. It is difficult to confirm that the nanoparticles are internalized rather than surface-bound but since they are not aligned with the edges of the collagen fibril it is likely that they are contained within the fibril. This indicates that nanoparticles, and therefore aptamers, are interspersed throughout the mineralized collagen and supports the conclusion that Aptamer G is playing a role in controlling intrafibrillar collagen mineralization.

We have demonstrated the differential influence that DNA aptamers can have on collagen mineralization based on essential factors of their secondary structure. Previous compelling examples exist where various forms of DNA such as poly-C nucleotides,[39] assembled DNA origami,[25–29] and native DNA[20–22] have been used to interact with and control mineral formation in vitro and in vivo. The recent work by Shen, et al.[21] demonstrates that very large native DNA can have a significant influence on collagen mineralization. In the same work, Shen, et al. showed that synthetic DNA could have a similar influence on collagen mineralization but in all

cases only considered double-stranded DNA without appreciable secondary structure or consideration for programmability. Here, we demonstrate the impressive potential of DNA secondary structure and the role that it can play when interacting with collagen and mineral precursors. A hypothesized mechanism of action is shown in Figure 5 where a DNA aptamer containing an adaptable G-quadruplex structure has an equilibrium-based interaction with collagen and calcium phosphate precursors. Aptamer conformation may change during this time due to interactions with calcium ions and collagen as noted in prior circular dichroism studies and in dynamic light scatter measurements presented here. This allows the aptamer to slow mineralization kinetics, seen in Figure 3A, while maintaining more than 80% of aptamer in solution, seen in Figure 3C. This may indicate an ability to shuttle calcium phosphate precursors into collagen fibrils while not being entrapped in the growing mineral. This promotes intrafibrillar mineralization of collagen similar to what has been reported using poly-aspartic acid additives and which is similar to bone-like structures. An aptamer containing a more rigid hairpin-loop structure has a non-equilibrium-based interaction with the collagen which appears to enhance its interaction with the collagen but limit its interaction with calcium-phosphate precursor structures in solution. This results in external mineralization of the collagen surface and a lack of intrafibrillar mineralization. These results provide new insight into the mechanism by which collagen may be mineralized in vivo including the role of non-collagenous proteins. This also demonstrates the effectiveness of Aptamer G as a biomimic of non-collagenous proteins that could be useful in influencing biomineralization in a biomedical setting. In future experiments, the structural aspects of DNA aptamers and the specific interaction with collagen should be further explored. The programmability and control available in DNA technology should also now be leveraged to further explore the potential of adaptable biomimetic DNA.

ASSOCIATED CONTENT

**Supporting Information**. Measurement of collagen fiber widths, additional SEM images and comparison to experiments using poly-aspartic acid, FT-IR relationship between peak intensities, Langmuir isotherm calculation and plot, gel electrophoresis of supernatant from mineralization experiments, dynamic light scattering of supernatant from mineralization experiments. The following files are available free of charge.

AUTHOR INFORMATION

**Corresponding Author**

*Aren E. Gerdon, gerdoar@emmanuel.edu, Ph. 617-735-9769

**Author Contributions**

The manuscript was written through contributions of all authors. All authors have given approval to the final version of the manuscript.

**Funding Sources**

Funding for this work was provided by Emmanuel College and the National Science Foundation DMR 1904460.

**Declaration of Competing Interest**

The authors declare that they have no known competing financial interests or personal relationships that could have appeared to influence the work reported in this paper.

ACKNOWLEDGMENT

The authors would like to thank Laurie Gower for recommendations on collagen preparation and for fruitful discussion. Electron Microscopy imaging, consultation, and/or services were performed in the Harvard Medical School (HMS) Electron Microscopy Facility.

REFERENCES

(1) Weiner, S.; Wagner, H. D. THE MATERIAL BONE: Structure-Mechanical Function Relations. *Annu. Rev. Mater. Sci.* **1998**, *28* (1), 271–298. https://doi.org/10.1146/annurev.matsci.28.1.271.
(2) Olszta, M. J.; Cheng, X.; Jee, S. S.; Kumar, R.; Kim, Y.-Y.; Kaufman, M. J.; Douglas, E. P.; Gower, L. B. Bone Structure and Formation: A New Perspective. *Mater. Sci. Eng. R Rep.* **2007**, *58* (3–5), 77–116. https://doi.org/10.1016/j.mser.2007.05.001.
(3) Jee, S.-S.; Thula, T. T.; Gower, L. B. Development of Bone-like Composites via the Polymer-Induced Liquid-Precursor (PILP) Process. Part 1: Influence of Polymer Molecular Weight. *Acta Biomater.* **2010**, *6* (9), 3676–3686. https://doi.org/10.1016/j.actbio.2010.03.036.
(4) Thula, T. T.; Svedlund, F.; Rodriguez, D. E.; Podschun, J.; Pendi, L.; Gower, L. B. Mimicking the Nanostructure of Bone: Comparison of Polymeric Process-Directing Agents. *Polymers* **2010**, *3* (1), 10–35. https://doi.org/10.3390/polym3010010.
(5) Thula, T. T.; Rodriguez, D. E.; Lee, M. H.; Pendi, L.; Podschun, J.; Gower, L. B. In Vitro Mineralization of Dense Collagen Substrates: A Biomimetic Approach toward the Development of Bone-Graft Materials. *Acta Biomater.* **2011**, *7* (8), 3158–3169. https://doi.org/10.1016/j.actbio.2011.04.014.
(6) Wingender, B.; Bradley, P.; Saxena, N.; Ruberti, J. W.; Gower, L. Biomimetic Organization of Collagen Matrices to Template Bone-like Microstructures. *Matrix Biol.* **2016**, *52–54*, 384–396. https://doi.org/10.1016/j.matbio.2016.02.004.
(7) Mukherjee, K.; Visakan, G.; Phark, J.-H.; Moradian-Oldak, J. Enhancing Collagen Mineralization with Amelogenin Peptide: Toward the Restoration of Dentin. *ACS Biomater. Sci. Eng.* **2020**, *6* (4), 2251–2262. https://doi.org/10.1021/acsbiomaterials.9b01774.
(8) Patel, A.; Zaky, S. H.; Schoedel, K.; Li, H.; Sant, V.; Beniash, E.; Sfeir, C.; Stolz, D. B.; Sant, S. Design and Evaluation of Collagen-Inspired Mineral-Hydrogel Nanocomposites for Bone Regeneration. *Acta Biomater.* **2020**, *112*, 262–273. https://doi.org/10.1016/j.actbio.2020.05.034.
(9) Al-Qudsy, L.; Hu, Y.-W.; Xu, H.; Yang, P.-F. Mineralized Collagen Fibrils: An Essential Component in Determining the Mechanical Behavior of Cortical Bone. *ACS Biomater. Sci. Eng.* **2023**, *9* (5), 2203–2219. https://doi.org/10.1021/acsbiomaterials.2c01377.
(10) Cuylear, D. L.; Elghazali, N. A.; Kapila, S. D.; Desai, T. A. Calcium Phosphate Delivery Systems for Regeneration and Biomineralization of Mineralized Tissues of the Craniofacial Complex. *Mol. Pharm.* **2023**, *20* (2), 810–828. https://doi.org/10.1021/acs.molpharmaceut.2c00652.

(11) Wang, J.; Liu, Q.; Guo, Z.; Pan, H.; Liu, Z.; Tang, R. Progress on Biomimetic Mineralization and Materials for Hard Tissue Regeneration. *ACS Biomater. Sci. Eng.* **2023**, *9* (4), 1757–1773. https://doi.org/10.1021/acsbiomaterials.1c01070.
(12) Oosterlaken, B. M.; Vena, M. P.; De With, G. In Vitro Mineralization of Collagen. *Adv. Mater.* **2021**, *33* (16), 2004418. https://doi.org/10.1002/adma.202004418.
(13) Gower, L. B. Biomimetic Model Systems for Investigating the Amorphous Precursor Pathway and Its Role in Biomineralization. *Chem. Rev.* **2008**, *108* (11), 4551–4627. https://doi.org/10.1021/cr800443h.
(14) Lausch, A. J.; Quan, B. D.; Miklas, J. W.; Sone, E. D. Extracellular Matrix Control of Collagen Mineralization In Vitro. *Adv. Funct. Mater.* **2013**, *23* (39), 4906–4912. https://doi.org/10.1002/adfm.201203760.
(15) Nudelman, F.; Lausch, A. J.; Sommerdijk, N. A. J. M.; Sone, E. D. In Vitro Models of Collagen Biomineralization. *J. Struct. Biol.* **2013**, *183* (2), 258–269. https://doi.org/10.1016/j.jsb.2013.04.003.
(16) Nurrohman, H.; Carneiro, K. M. M.; Hellgeth, J.; Saeki, K.; Marshall, S. J.; Marshall, G. W.; Habelitz, S. The Role of Protease Inhibitors on the Remineralization of Demineralized Dentin Using the PILP Method. *PLOS ONE* **2017**, *12* (11), e0188277. https://doi.org/10.1371/journal.pone.0188277.
(17) Ma, Y.; Hoff, S. E.; Huang, X.; Liu, J.; Wan, Q.; Song, Q.; Gu, J.; Heinz, H.; Tay, F. R.; Niu, L. Involvement of Prenucleation Clusters in Calcium Phosphate Mineralization of Collagen. *Acta Biomater.* **2021**, *120*, 213–223. https://doi.org/10.1016/j.actbio.2020.07.038.
(18) Tang, L.; Zhu, L.; Liu, Y.; Zhang, Y.; Li, B.; Wang, M. Crosslinking Improve Demineralized Dentin Performance and Synergistically Promote Biomimetic Mineralization by CaP_PILP. *ACS Omega* **2023**, *8* (16), 14410–14419. https://doi.org/10.1021/acsomega.2c07825.
(19) Coscas, R.; Bensussan, M.; Jacob, M.-P.; Louedec, L.; Massy, Z.; Sadoine, J.; Daudon, M.; Chaussain, C.; Bazin, D.; Michel, J.-B. Free DNA Precipitates Calcium Phosphate Apatite Crystals in the Arterial Wall in Vivo. *Atherosclerosis* **2017**, *259*, 60–67. https://doi.org/10.1016/j.atherosclerosis.2017.03.005.
(20) Qin, Z.; Wang, C.; Zhang, J.; Wang, Z.; Wei, Y.; Li, Y.; Dai, S.; Tay, F. R.; Niu, L. DNA-Based Materials Inspired by Natural Extracellular DNA. *Adv. Funct. Mater.* **2023**, *33* (31), 2211669. https://doi.org/10.1002/adfm.202211669.
(21) Shen, M.; Jiao, K.; Wang, C.; Ehrlich, H.; Wan, M.; Hao, D.; Li, J.; Wan, Q.; Tonggu, L.; Yan, J.; Wang, K.; Ma, Y.; Chen, J.; Tay, F. R.; Niu, L. Extracellular DNA: A Missing Link in the Pathogenesis of Ectopic Mineralization. *Adv. Sci.* **2022**, *9* (5), 2103693. https://doi.org/10.1002/advs.202103693.
(22) Dick, T. A.; Sone, E. D.; Uludağ, H. Mineralized Vectors for Gene Therapy. *Acta Biomater.* **2022**, *147*, 1–33. https://doi.org/10.1016/j.actbio.2022.05.036.
(23) Wang, C.; Qin, Z.; Wei, Y.; Hao, J.; Zhu, Y.; Zhao, F.; Jiao, K.; Ehrlich, H.; Tay, F. R.; Niu, L. The Immunomodulatory Effects of RNA-Based Biomaterials on Bone Regeneration. *Acta Biomater.* **2023**, *162*, 32–43. https://doi.org/10.1016/j.actbio.2023.03.031.
(24) Lukeman, P. S.; Stevenson, M. L.; Seeman, N. C. Morphology Change of Calcium Carbonate in the Presence of Polynucleotides. *Cryst. Growth Des.* **2008**, *8* (4), 1200–1202. https://doi.org/10.1021/cg700656r.
(25) Han, L.; Jin, C.; Liu, B.; Che, S. DNA–Silica Mineralization: The Formation of Exceptional Two Dimensional-Square *p* 4 *Mm* Symmetry by a Structural Transformation. *Chem. Mater.* **2012**, *24* (3), 504–511. https://doi.org/10.1021/cm202874w.

(26) Nguyen, L.; Döblinger, M.; Liedl, T.; Heuer-Jungemann, A. DNA-Origami-Templated Silica Growth by Sol–Gel Chemistry. *Angew. Chem. Int. Ed.* **2019**, *58* (3), 912–916. https://doi.org/10.1002/anie.201811323.
(27) Athanasiadou, D.; Carneiro, K. M. M. DNA Nanostructures as Templates for Biomineralization. *Nat. Rev. Chem.* **2021**, *5* (2), 93–108. https://doi.org/10.1038/s41570-020-00242-5.
(28) Danesi, A. L.; Athanasiadou, D.; Aderinto, A. O.; Rasie, P.; Chou, L. Y. T.; Carneiro, K. M. M. Peptide-Decorated DNA Nanostructures Promote Site-Specific Hydroxyapatite Growth. *ACS Appl. Mater. Interfaces* **2022**, *14* (1), 1692–1698. https://doi.org/10.1021/acsami.1c19271.
(29) Wu, S.; Zhang, M.; Song, J.; Weber, S.; Liu, X.; Fan, C.; Wu, Y. Fine Customization of Calcium Phosphate Nanostructures with Site-Specific Modification by DNA Templated Mineralization. *ACS Nano* **2021**, *15* (1), 1555–1565. https://doi.org/10.1021/acsnano.0c08998.
(30) Athanasiadou, D.; Meshry, N.; Monteiro, N. G.; Ervolino Silva, A. C.; Chan, R. L.; McCulloch, C. A.; Okamoto, R.; Carneiro, K. M. M. DNA Hydrogels for Bone Regeneration. *Proc. Natl. Acad. Sci.* **2023**, *120* (17), e2220565120. https://doi.org/10.1073/pnas.2220565120.
(31) Feagin, T. A.; Maganzini, N.; Soh, H. T. Strategies for Creating Structure-Switching Aptamers. *ACS Sens.* **2018**, *3* (9), 1611–1615. https://doi.org/10.1021/acssensors.8b00516.
(32) Keefe, A. D.; Pai, S.; Ellington, A. Aptamers as Therapeutics. *Nat. Rev. Drug Discov.* **2010**, *9* (7), 537–550. https://doi.org/10.1038/nrd3141.
(33) Yüce, M.; Ullah, N.; Budak, H. Trends in Aptamer Selection Methods and Applications. *The Analyst* **2015**, *140* (16), 5379–5399. https://doi.org/10.1039/C5AN00954E.
(34) Bawazer, L. A.; Newman, A. M.; Gu, Q.; Ibish, A.; Arcila, M.; Cooper, J. B.; Meldrum, F. C.; Morse, D. E. Efficient Selection of Biomineralizing DNA Aptamers Using Deep Sequencing and Population Clustering. *ACS Nano* **2014**, *8* (1), 387–395. https://doi.org/10.1021/nn404418s.
(35) Wei, Y.; Chen, M.; Li, M.; Wang, D.; Cai, K.; Luo, Z.; Hu, Y. Aptamer/Hydroxyapatite-Functionalized Titanium Substrate Promotes Implant Osseointegration via Recruiting Mesenchymal Stem Cells. *ACS Appl. Mater. Interfaces* **2022**, *14* (38), 42915–42930. https://doi.org/10.1021/acsami.2c10809.
(36) Zhou, L.; Chen, Z.; Dong, K.; Yin, M.; Ren, J.; Qu, X. DNA-Mediated Biomineralization of Rare-Earth Nanoparticles for Simultaneous Imaging and Stimuli-Responsive Drug Delivery. *Biomaterials* **2014**, *35* (30), 8694–8702. https://doi.org/10.1016/j.biomaterials.2014.06.034.
(37) Liu, B.; Liu, J. Comprehensive Screen of Metal Oxide Nanoparticles for DNA Adsorption, Fluorescence Quenching, and Anion Discrimination. *ACS Appl. Mater. Interfaces* **2015**, *7* (44), 24833–24838. https://doi.org/10.1021/acsami.5b08004.
(38) Ozaki, M.; Nagai, K.; Nishiyama, H.; Tsuruoka, T.; Fujii, S.; Endoh, T.; Imai, T.; Tomizaki, K.; Usui, K. Site-Specific Control of Silica Mineralization on DNA Using a Designed Peptide. *Chem. Commun.* **2016**, *52* (21), 4010–4013. https://doi.org/10.1039/C5CC07870A.
(39) Lu, C.; Huang, Z.; Liu, B.; Liu, Y.; Ying, Y.; Liu, J. Poly-cytosine DNA as a High-Affinity Ligand for Inorganic Nanomaterials. *Angew. Chem. Int. Ed.* **2017**, *56* (22), 6208–6212. https://doi.org/10.1002/anie.201702998.

(40) Wang, L.; Zhang, Z.; Liu, B.; Liu, Y.; Lopez, A.; Wu, J.; Liu, J. Interfacing DNA Oligonucleotides with Calcium Phosphate and Other Metal Phosphates. *Langmuir* **2018**, *34* (49), 14975–14982. https://doi.org/10.1021/acs.langmuir.7b03204.

(41) Wang, Y.; Reddy Satyavolu, N. S.; Lu, Y. Sequence-Specific Control of Inorganic Nanomaterials Morphologies by Biomolecules. *Curr. Opin. Colloid Interface Sci.* **2018**, *38*, 158–169. https://doi.org/10.1016/j.cocis.2018.10.009.

(42) Zhou, Y.; Huang, Z.; Yang, R.; Liu, J. Selection and Screening of DNA Aptamers for Inorganic Nanomaterials. *Chem. – Eur. J.* **2018**, *24* (11), 2525–2532. https://doi.org/10.1002/chem.201704600.

(43) Baillargeon, K. R.; Meserve, K.; Faulkner, S.; Watson, S.; Butts, H.; Deighan, P.; Gerdon, A. E. Precipitation SELEX: Identification of DNA Aptamers for Calcium Phosphate Materials Synthesis. *Chem. Commun.* **2017**, *53* (6), 1092–1095. https://doi.org/10.1039/C6CC08687J.

(44) Colon, S.; Paige, A.; Bolarinho, R.; Young, H.; Gerdon, A. E. Secondary Structure of DNA Aptamer Influences Biomimetic Mineralization of Calcium Carbonate. *ACS Appl. Mater. Interfaces* **2023**, *15* (5), 6274–6282. https://doi.org/10.1021/acsami.2c15626.

(45) Burge, S.; Parkinson, G. N.; Hazel, P.; Todd, A. K.; Neidle, S. Quadruplex DNA: Sequence, Topology and Structure. *Nucleic Acids Res.* **2006**, *34* (19), 5402–5415. https://doi.org/10.1093/nar/gkl655.

(46) Shlaferman, J.; Paige, A.; Meserve, K.; Miech, J. A.; Gerdon, A. E. Selected DNA Aptamers Influence Kinetics and Morphology in Calcium Phosphate Mineralization. *ACS Biomater. Sci. Eng.* **2019**, *5* (7), 3228–3236. https://doi.org/10.1021/acsbiomaterials.9b00308.

(47) Gustafsson, J. P. Visual MINTEQ 2013.

(48) Vasconcellos, K. B.; McHugh, S. M.; Dapsis, K. J.; Petty, A. R.; Gerdon, A. E. Biomimetic Nanoparticles with Polynucleotide and PEG Mixed-Monolayers Enhance Calcium Phosphate Mineralization. *J. Nanoparticle Res.* **2013**, *15* (9), 1942. https://doi.org/10.1007/s11051-013-1942-5.

(49) Schaaff, T. G.; Knight, G.; Shafigullin, M. N.; Borkman, R. F.; Whetten, R. L. Isolation and Selected Properties of a 10.4 kDa Gold:Glutathione Cluster Compound. *J. Phys. Chem. B* **1998**, *102* (52), 10643–10646. https://doi.org/10.1021/jp9830528.

(50) Schaaff, T. G.; Whetten, R. L. Giant Gold−Glutathione Cluster Compounds: Intense Optical Activity in Metal-Based Transitions. *J. Phys. Chem. B* **2000**, *104* (12), 2630–2641. https://doi.org/10.1021/jp993691y.

(51) Hostetler, M. J.; Templeton, A. C.; Murray, R. W. Dynamics of Place-Exchange Reactions on Monolayer-Protected Gold Cluster Molecules. *Langmuir* **1999**, *15* (11), 3782–3789. https://doi.org/10.1021/la981598f.

(52) Walters, M. A.; Leung, Y. C.; Blumenthal, N. C.; Konsker, K. A.; LeGeros, R. Z. A Raman and Infrared Spectroscopic Investigation of Biological Hydroxyapatite. *J. Inorg. Biochem.* **1990**, *39* (3), 193–200. https://doi.org/10.1016/0162-0134(90)84002-7.

(53) Choi, S.; Coonrod, S.; Estroff, L.; Fischbach, C. Chemical and Physical Properties of Carbonated Hydroxyapatite Affect Breast Cancer Cell Behavior. *Acta Biomater.* **2015**, *24*, 333–342. https://doi.org/10.1016/j.actbio.2015.06.001.

(54) Gerdon, A. E.; Wright, D. W.; Cliffel, D. E. Quartz Crystal Microbalance Characterization of Nanostructure Assemblies in Biosensing. In *Nanotechnologies for the Life Sciences*; Kumar, C. S. S. R., Ed.; Wiley-VCH Verlag GmbH & Co. KGaA: Weinheim, Germany, 2007; p ntls0026. https://doi.org/10.1002/9783527610419.ntls0026.

(55) Connelly, C.; Cicuto, T.; Leavitt, J.; Petty, A.; Litman, A.; Margolis, H. C.; Gerdon, A. E. Dynamic Interactions of Amelogenin with Hydroxyapatite Surfaces Are Dependent on Protein Phosphorylation and Solution pH. *Colloids Surf. B Biointerfaces* **2016**, *148*, 377–384. https://doi.org/10.1016/j.colsurfb.2016.09.010.

Figure Captions

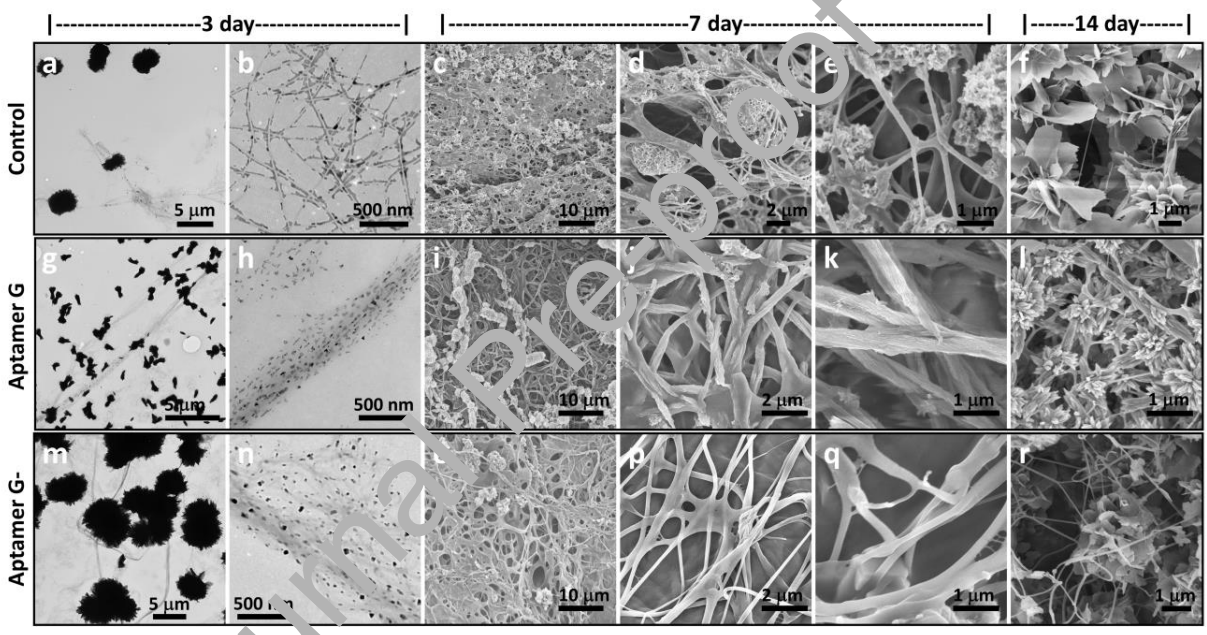


**Figure 1**. TEM and SEM images of collagen hydrogels mineralized with calcium phosphate in the presence or absence of DNA aptamers. a-f) Control experiments in the absence of DNA aptamers shows mineral external to the collagen fibers after 3 days of reaction in a,b using TEM, external mineralization or mineral formed between fibers after 7 days of reaction in c-e and after 14 days of reaction for f using SEM. g-l) Mineralization using DNA Aptamer G appears to produce smaller, bundle-like mineral particles and mineral associated with the long axis of collagen fibers indicating early signs of intrafibrillar mineralization after 3 days of reaction in g,h using TEM, fibrils that are thick and rigid, indicating intrafibrillar mineralization after 7 days of reaction for i-k and after 14 days of reaction for l using SEM. m-r) Mineralization using DNA Aptamer G- shows mineralization similar to the control with external or surface mineralization after 3 days of reaction in m,n using TEM, 7 days of reaction for o-q and after 14 days of reaction for r.

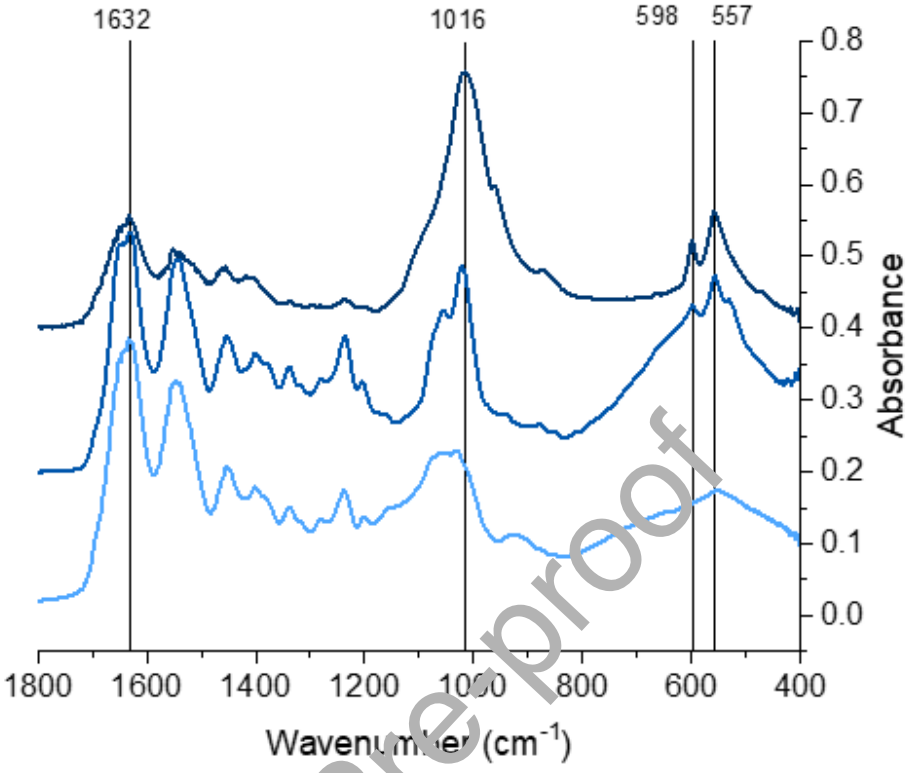


**Figure 2.** FT-IR spectroscopy analysis of three replicate, representative lyophilized collagen samples mineralized with calcium phosphate in the presence of Aptamer G for 7 days. Three spectra show the presence of calcium phosphate and collagen in all three examples but show different levels of crystallinity. This is observed in variability in amide peak intensity related to collagen (1632 $cm^{-1}$), phosphate peak intensity related to mineral (1016 $cm^{-1}$), and phosphate peaks related to crystallinity (557 $cm^{-1}$ and 598 $cm^{-1}$).

A

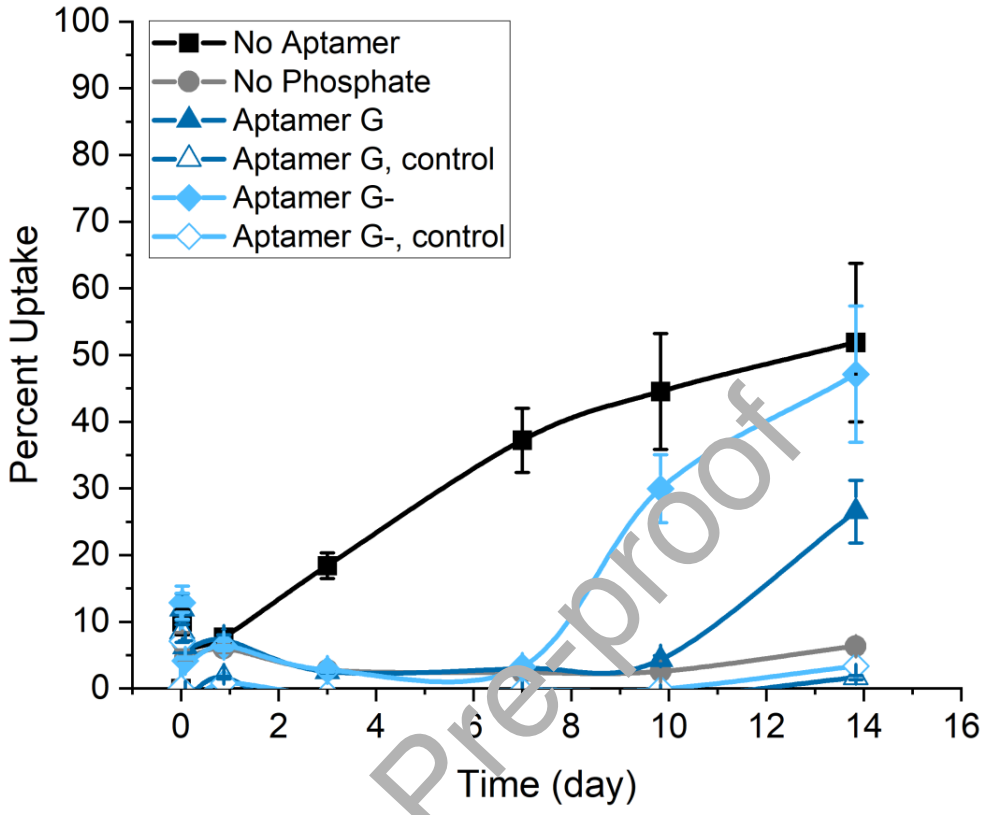

B

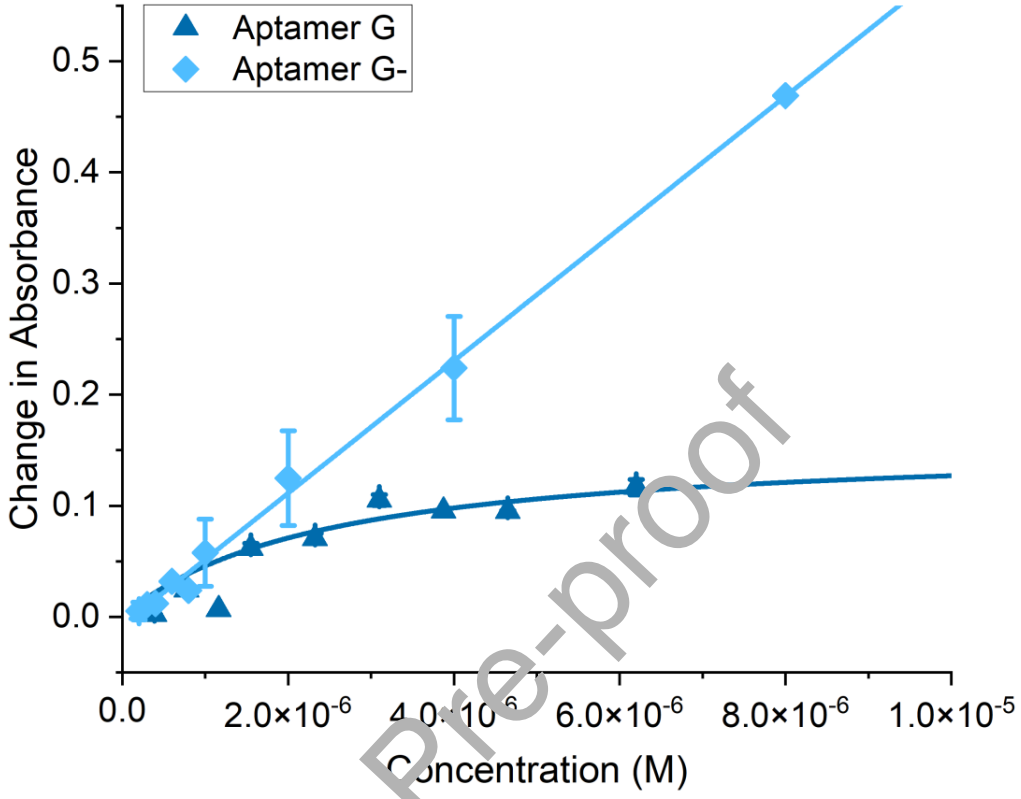

C

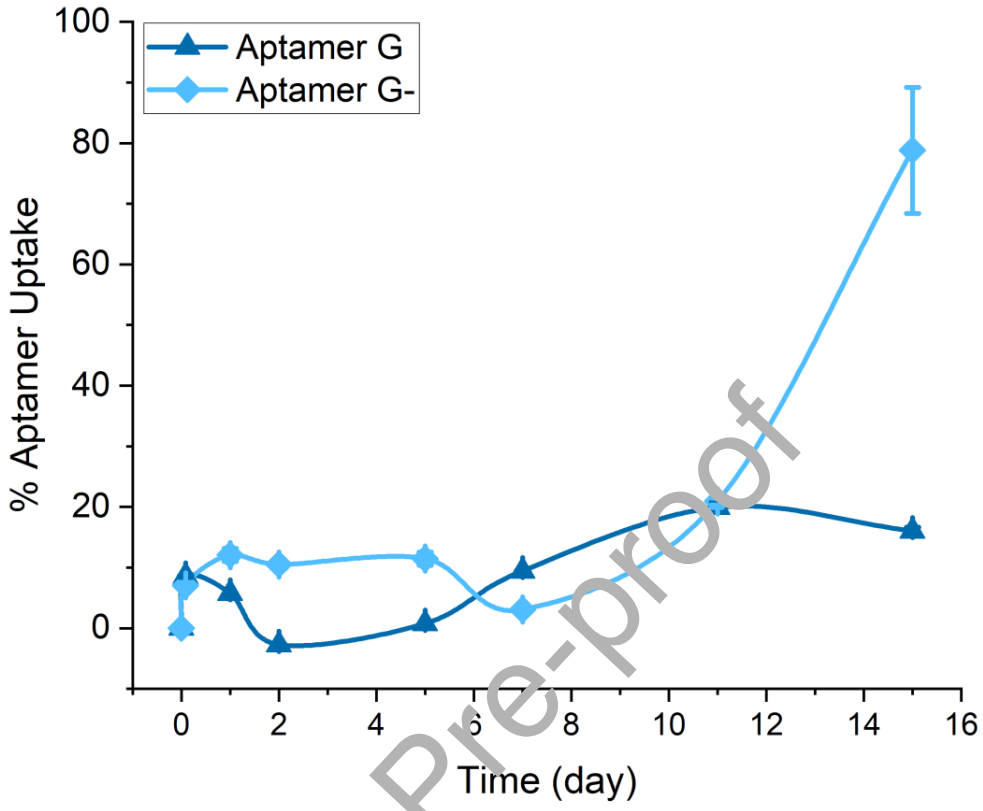


**Figure 3**. Analysis of calcium [illegible]ptamer interaction with collagen. A) Calcium uptake in collagen or bulk solution mi[illegible]ation measured by the decrease in calcium ion concentration in solution by ion selective electrode. With no phosphate present, a small amount of calcium ion is apparently absorbed by the collagen hydrogel. In the absence of aptamer, mineralization proceeds on the timeframe of 1-3 days but with aptamer present mineralization is delayed by 7-10 days. Error bars represent standard deviation propagated through replicate standard curves. At 7 days, both Aptamer G and Aptamer G- are statistically different from the No Aptamer control ($P < 0.0005$). At 14 days, Aptamer G is statistically different from Aptamer G- and the No Aptamer control ($P < 0.05$). B) DNA aptamer interaction with collagen in the presence of calcium at different concentrations of aptamer. Error bars show standard deviation of replicate measurement. C) DNA aptamer interaction with collagen during calcium phosphate mineralization over a 14-day reaction. Error bars show standard deviation of replicate measurements. At both 7 and 14 days, differences between Aptamer G and Aptamer G- are statistically different ($P < 0.0005$).

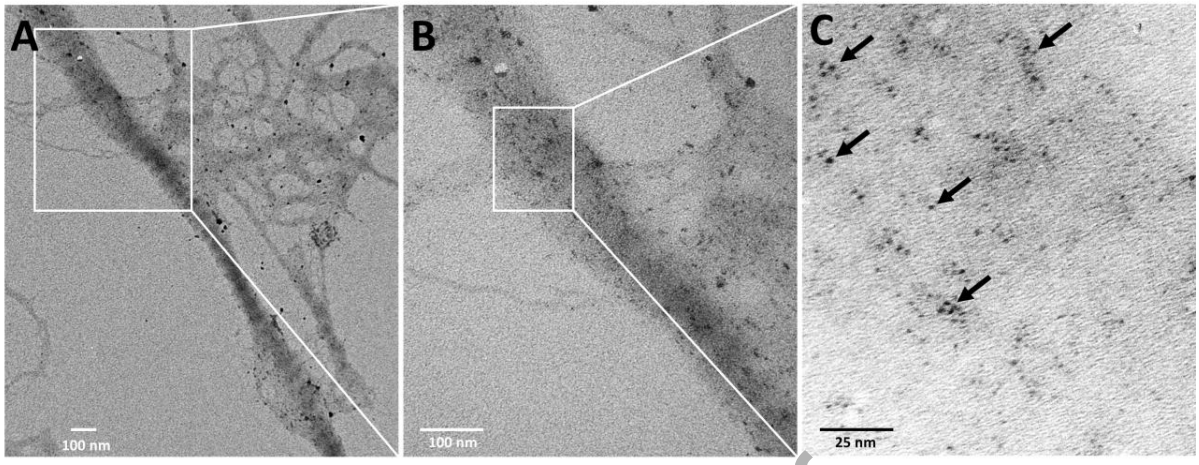


**Figure 4.** TEM images of collagen fibers mineralized in calcium phosphate for 7 days with Aptamer G and Aptamer G conjugated gold nanoparticles. Figures B and C are higher magnification images of sections of Figure A. Arrows have been added in C to point out the small, 2 nm gold nanoparticles present in the collagen fiber.

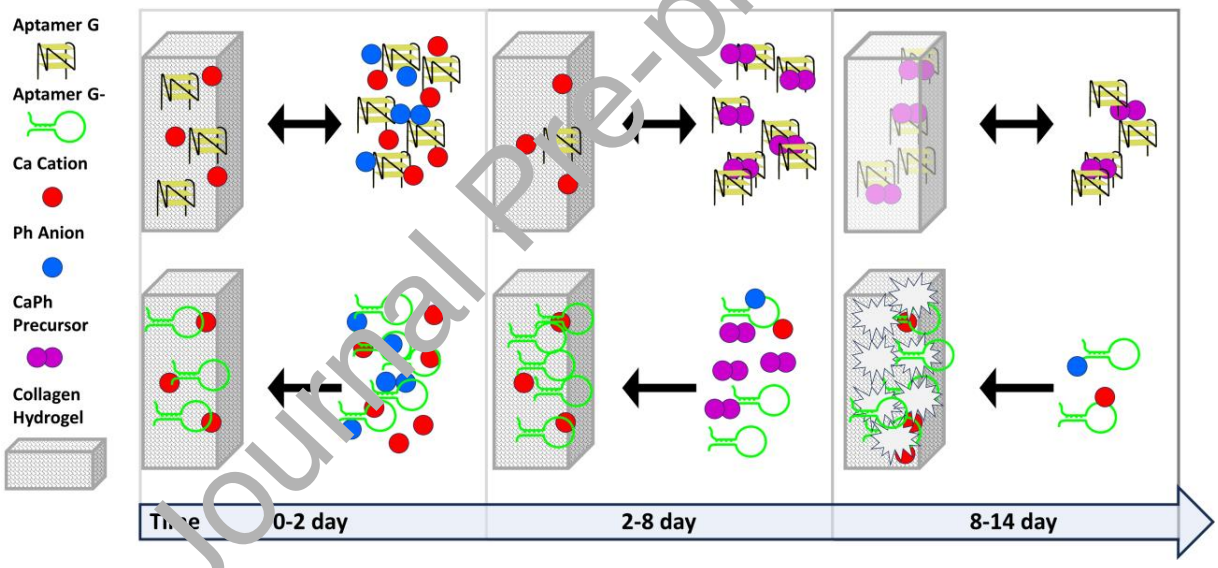


**Figure 5.** Schematic demonstrating the hypothesis of mode of action of DNA aptamers when influencing calcium phosphate mineralization of collagen. Aptamer G results in intrafibrillar mineralization of collagen due to an equilibrium interaction established between the aptamer, collagen, and calcium phosphate precursors. Aptamer G- results in external mineralization of the collagen surface due to non-equilibrium adsorption of aptamer to collagen and lack of control of mineralization precursors.

**Statement of Significance**

Collagen is the protein structural component that mineralizes with calcium phosphate to form durable bone. Crystalline calcium phosphate must be infused throughout the collagen fiber structure to produce a strong material. This process is assisted by soluble proteins that interact with both calcium phosphate precursors and the collagen protein and has been proposed to follow a polymer-induce liquid precursor (PILP) model. Further understanding of this model and control of the process through synthetic, biomimetic molecules could have significant advantages in biomedical, restorative procedures. For the first time, synthetic DNA aptamers with specific secondary structures are here shown to influence and direct collagen mineralization. The mechanism of this process has been studied to demonstrate an important equilibrium between the DNA aptamer, calcium phosphate precursors, and collagen.

**Graphical Abstract**

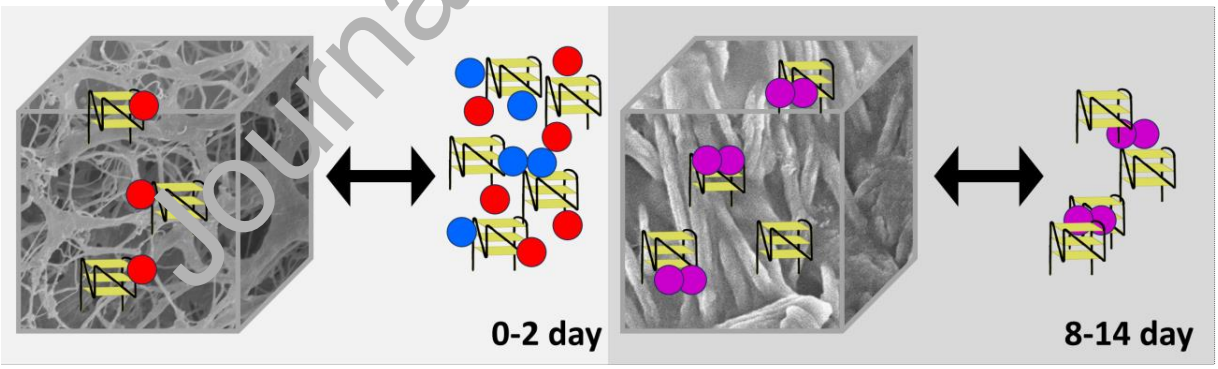

**Declaration of Interests**

☐The authors declare that they have no known competing financial interests or personal relationships that could have appeared to influence the work reported in this paper.

☒The authors declare the following financial interests/personal relationships which may be considered as potential competing interests:

Aren E. Gerdon reports financial support was provided by National Science Foundation.